ARTICLES

Preparation and Fluorescence Spectroscopy of Bulk Monoclinic Eu^{3+}:Y_2O_3 and Comparison to Eu^{3+}:Y_2O_3 Nanocrystals

Diane K. Williams, Bipin Bihari, and Brian M. Tissue*

Department of Chemistry, Virginia Polytechnic Institute and State University, Blacksburg, Virginia 24061-0212

James M. McHale

Princeton Materials Institute, Princeton University, Princeton, New Jersey 08544-1003

Received: September 12, 1997

We report the laser spectroscopic characterization of bulk monoclinic Eu^{3+}:Y_2O_3, which was prepared by a high-temperature, high-pressure synthesis method. The bulk monoclinic phase has sharp spectral lines without the line broadening and "secondary phase" of Eu^{3+}:Y_2O_3 nanocrystals. The unusual optical properties of site A in this material have been determined to be intrinsic to the monoclinic phase and are not a result of surface effects in the nanocrystals. The $^5D_0$ fluorescence lifetimes are longer in the nanocrystals than in the bulk material, indicating that there is no lifetime shortening in the nanocrystals due to quenching by the proximity of surface defects.

1. Introduction

The development of new types of flat panel and projection displays has created a need for optical phosphors with new or enhanced properties.[1] Nanophase and nanocrystalline materials, typically defined as polycrystalline solids with particle diameters of 100 nm or less, offer new possibilities for advanced phosphor applications. Nanocrystals can form in new phases[2] or exhibit enhanced structural, electronic, and optical properties.[3−5] Lanthanide-doped cubic-phase Y_2O_3 and related materials are common phosphors in optical display and lighting applications,[6] and the search for new phosphors has led to the preparation of nanocrystalline forms of Y_2O_3.[7−10] Preparing nanocrystalline Y_2O_3 by gas-phase condensation results in the formation of the monoclinic crystal structure,[8,11,12] rather than the usual cubic structure.[13] Optical studies of 23 nm monoclinic Eu^{3+}:Y_2O_3 showed several anomalies in the optical spectra and fluorescence dynamics.[8] As a result, we initiated this study to prepare and characterize bulk monoclinic Eu^{3+}:Y_2O_3 to provide the baseline information for understanding the nanocrystalline material. In this paper, we present the optical spectra and fluorescence dynamics of bulk monoclinic Eu^{3+}:Y_2O_3 prepared by a high-temperature, high-pressure method; we also compare these results to the optical behavior of nanocrystalline Eu^{3+}:Y_2O_3 prepared by gas-phase condensation.[8] The results will indicate which features in the optical results of nanocrystalline Eu^{3+}:Y_2O_3 are intrinsic to monoclinic Eu^{3+}:Y_2O_3 and which features are probably due to the large surface-to-volume ratio of the nanocrystals.

Eu_2O_3 through Dy_2O_3 in the lanthanide series can form in the monoclinic structure at high temperature or high pressure,[13−15] but Y_2O_3 and lanthanide sesquioxides with an ionic radius smaller than that of Dy_2O_3 require both high temperature and high pressure.[14] The monoclinic phase of these sesquioxides has space group $C2/m$, and the lattice possesses three crystallographically distinct cation sites, each having point group symmetry C_s.[16,18] All three cation sites are 7-fold coordinated. The coordination of two cation sites (Ln I and Ln II) can be described by six oxygens at the apexes of a trigonal prism with a seventh oxygen lying along the normal to a face. The coordination of the third site (Ln III) is described as a distorted octahedron with a seventh oxygen at a long distance (3.13 Å for Eu_2O_3).[14,16−18] Formation of nanocrystalline Y_2O_3 in the monoclinic phase at ambient conditions has been attributed to an additional hydrostatic pressure component, resulting from the Gibbs−Thomson effect.[11] Recent results suggest that Y_2O_3 prepared by gas-phase condensation forms in the monoclinic phase for particle diameters in the 10−30 nm range, but that particles of approximately 5 nm form in the usual cubic phase, although with extensive disorder.[19] This result suggests that some other factor controls the overall crystal structure at very small particle sizes.

Optical spectroscopy studies of bulk monoclinic lanthanide sesquioxides have been limited to Eu_2O_3[15,20] and Eu^{3+}:Gd_2O_3.[18,21] The Eu^{3+} ion occupies the three nonequivalent crystallographic sites in the monoclinic structure, producing three distinct sets of optical spectra. Theoretical energy level splittings for the $7F_J$ energy levels were generated from ab initio calculation of the crystal-field parameters for each cation site in monoclinic Eu^{3+}:Gd_2O_3.[18] These calculations indicated that the three distinct sets of optical spectra, labeled sites A, B, and C, correspond to cation sites Ln III, Ln II, and Ln I, respectively.

The optical spectra of nanocrystalline Eu_2O_3 and Eu^{3+}:Y_2O_3 have the same overall energy level splitting pattern for the three

* Corresponding author. Phone: (540) 231−3786. Fax: (540) 231−3255. E-mail: tissue@vt.edu.

S1089-5647(97)02996-9 CCC: $15.00
Published on Web 01/16/1998

cation sites as in the bulk monoclinic Eu_2O_3 and Eu^{3+}:Gd_2O_3. However, the spectral lines of the nanocrystals appeared to be broadened, and a "secondary phase" increases in dominance as the particle diameter becomes smaller.[7] The nanocrystalline 0.1% Eu^{3+}:Y_2O_3 showed weak energy transfer from site A to sites B and C, but not between sites B and C. Site A also showed more lines than expected in the fluorescence spectra, non-single-exponential fluorescence decay from the $^5D_0$ level, and a shorter $^5D_1$ lifetime than sites B and C.[8] Because of the high Eu^{3+} concentration in earlier bulk material studies, Eu_2O_3 and 5% Eu^{3+}:Gd_2O_3,[18] excitation energy migrated rapidly between all sites. The high concentration prevents a direct comparison of the fluorescence dynamics of the nanocrystalline 0.1% Eu^{3+}:Y_2O_3 with previously studied bulk material.

2. Experimental Section

The bulk Eu^{3+}:Y_2O_3 sample was prepared by dissolving 3.239×10^{-2} mol $Y(NO_3)_3 \cdot 6H_2O$ (Johnson Matthey, 99.9%) and 1.6×10^{-5} mol Eu_2O_3 (Aldrich, 99.95+%) in 100 mL of distilled H_2O and 1 mL of ~70% HNO_3(aq). A hydrous oxide gel precipitated from this solution by adding NH_4OH. The gel was filtered, and the precipitate was washed several times with distilled H_2O, and then calcined at 1000 °C for 24 h to produce Eu^{3+}:Y_2O_3 with the cubic structure. This material was transformed to the monoclinic structure by application of high pressure and high temperature. Approximately 50 mg of the calcined Eu^{3+}:Y_2O_3 was loaded into a 10 mm segment of 3 mm i.d. Pt tubing, which was then welded closed on both ends. The tubing was then loaded into a Quick Press piston cylinder apparatus (Depths of the Earth Co.) and heated from 30 to 1100 °C while the pressure was slowly increased to 25 kbar. The pressure medium was pyrophyllite. The sample was maintained at 25 kbar and 1100 °C for 1 h and then was quenched to room temperature in approximately 1 min. The pressure was released slowly, and the sample was extracted from the Pt capsule. The resulting material was identified as monoclinic Eu^{3+}:Y_2O_3 from the powder X-ray diffraction pattern.[22]

The nanocrystalline Eu^{3+}:Y_2O_3 was prepared by a gas-phase condensation technique using CO2-laser vaporization of ceramic pellets.[7,8,12] Pressed and sintered pellets of 0.1% Eu^{3+}:Y_2O_3 were vaporized in a nitrogen atmosphere at 400 Torr. The nanocrystalline particles collected on a cold finger filled with 50−60 °C water, which kept the quenching temperature fairly constant. The phase and particle sizes of the nanocrystalline material were characterized by transmission electron microscopy (TEM) and powder X-ray diffraction (XRD). The particle sizes were determined from X-ray diffraction line widths using the Scherrer equation[23] and from a survey of the TEM micrographs.

For optical spectroscopy, the materials were packed into a depression on a copper sample holder, which was mounted on the cold head of a closed-cycle refrigerator (Cryomech GB 15). All of the spectra were recorded at a sample temperature of approximately 13 K. All spectra and decay transients were recorded using a Nd^{3+}:YAG-pumped dye laser with Coumarin 540A dye as the excitation source. Excitation spectra were recorded by scanning the laser and monitoring fluorescence with a 0.25 m monochromator with a band-pass of 6 nm and a photomultiplier tube (Hammamatsu P-28). Fluorescence spectra were recorded by tuning the laser to an excitation line and scanning a 1 m monochromator (Spex l000M) that was equipped with a cooled GaAs photomultiplier tube (Hammamatsu R-636). The photomultiplier signals were processed with a boxcar averager (Stanford SR250) and stored using an analog-to-digital data-acquisition board (National Instruments Lab-PC+) and LabView computer program. Fluorescence transients were recorded with a 350 MHz digital oscilloscope (Tektronix TDS460) after typically averaging 200 laser shots.

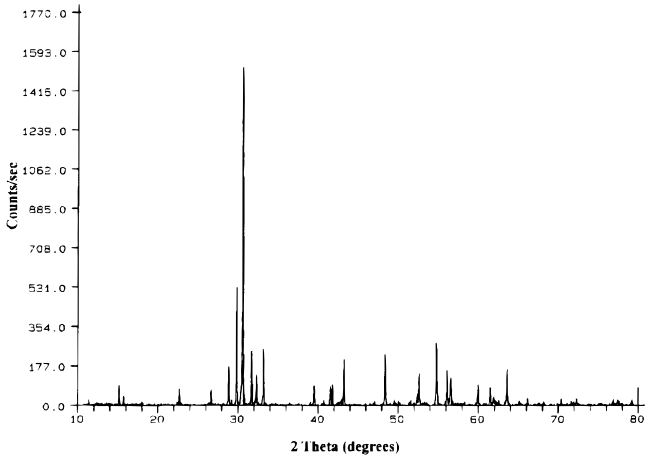

Figure 1. Powder X-ray diffraction pattern of bulk monoclinic 0.1% Eu^{3+}:Y_2O_3 prepared by the high-pressure, high-temperature method.

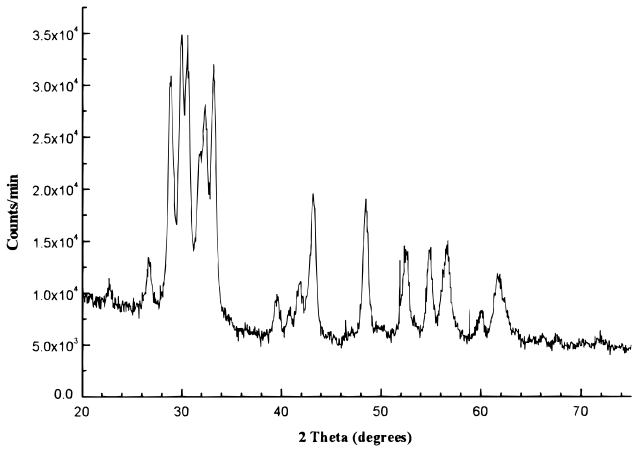

Figure 2. Powder X-ray diffraction pattern of nanocrystalline monoclinic 0.1% Eu^{3+}:Y_2O_3 prepared by gas-phase condensation.

3. Results and Discussion

Figure 1 shows the powder X-ray diffraction pattern of the bulk monoclinic 0.1% Eu^{3+}:Y_2O_3 sample. The line positions match the published diffraction pattern for monoclinic Y_2O_3,[22] with the exception of three small unassigned reflections at $2\theta = 41.5$, 52.7, and 56.2°. Figure 2 shows the powder X-ray diffraction pattern of nanocrystalline 0.1% Eu^{3+}:Y_2O_3. There are no lines due to the presence of cubic Y_2O_3 in either of these diffraction patterns. Broad-band excitation spectra were recorded monitoring fluorescence at approximately 611 nm, which is the strongest fluorescence line in cubic Eu^{3+}:Y_2O_3. The fluorescence spectroscopy is much more sensitive than X-ray diffraction to the presence of secondary phases, confirming that neither bulk nor nanocrystalline samples contained cubic Eu^{3+}:Y_2O_3.

The powder XRD pattern in Figure 2 is essentially identical with respect to line positions, line widths, and relative intensities to the powder pattern of submicrometer powder prepared by thermal plasma processing with an average diameter of approximately 21 nm.[22] The diffraction lines of the nanocrystalline material are broadened due to the small particle size. The average particle diameter calculated from the XRD line widths using the Scherrer equation was 23 nm, which was consistent

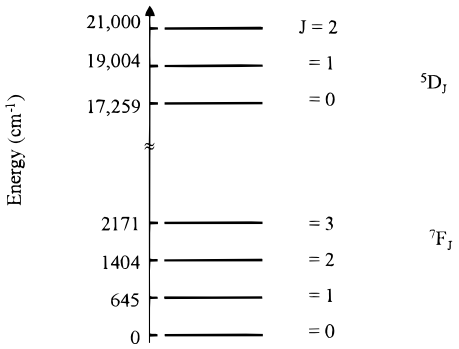

Figure 3. Partial energy level diagram of the Eu^{3+} ion in solids. Each level can be split into $2J + 1$ sublevels.

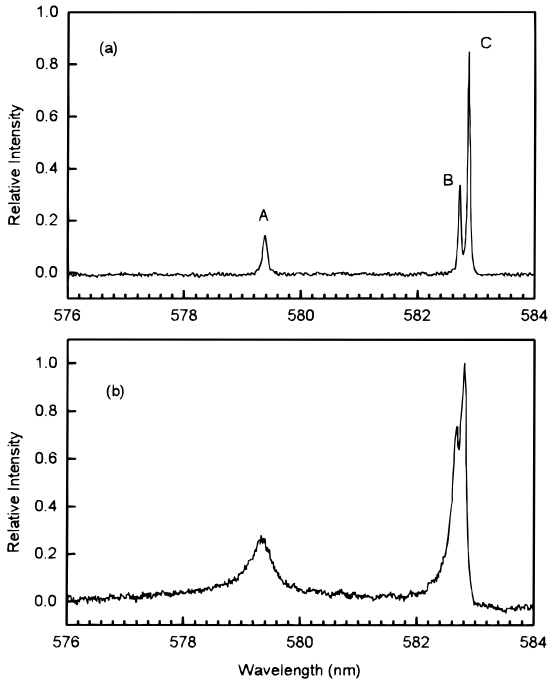

Figure 4. $^7F_0 \rightarrow {}^5D_0$ excitation spectra of (a) bulk monoclinic 0.1% Eu^{3+}:Y_2O_3 and (b) nanocrystalline 0.1% Eu^{3+}:Y_2O_3. The 0.25 m monochromator was set at 624.1 nm, and the boxcar delay and gate width were 20 μs and 150 μs, respectively. The *y*-axis for all spectra and transients in this paper is fluorescence intensity in arbitrary units.

with the 7−30 nm range of particle diameters observed in TEM micrographs. The only major difference between the bulk and nanocrystalline diffraction patterns was the difference in relative intensity of the reflection at $2\theta = 30.7°$.

Figure 3 shows a partial energy level diagram of the Eu^{3+} ion in a solid host. The overall energy level structure of the Eu^{3+} ion does not change in different hosts due to the shielding of the 4f electrons by outer shell 5s and 5p electrons.[24] Each energy level shown in Figure 3 can be split into $2J + 1$ sublevels, and this fine structure is sensitive to the local crystalline field surrounding the Eu^{3+} ion. Therefore, distinct spectra arise from Eu^{3+} ions in different crystallographic cation sites. The spectra in this paper follow the site A, B, and C labeling notation, as in refs 18 and 20.

Figure 4a shows the $^7F_0 \rightarrow {}^5D_0$ excitation spectrum of the bulk monoclinic Eu^{3+}:Y_2O_3. There are three sharp lines at 579.39, 582.72, and 582.87 nm, corresponding to sites A, B, and C, respectively. Figure 4b shows the analogous $^7F_0 \rightarrow {}^5D_0$ excitation spectrum of the nanocrystalline Eu^{3+}:Y_2O_3. Parts a and b of Figure 5 show the $^7F_0 - {}^5D_1$ excitation spectra of the bulk monoclinic Eu^{3+}:Y_2O_3 and Eu^{3+}:Y_2O_3 nanocrystals, respectively. In the bulk material spectrum, the excitation lines at 526.09 and 527.31 nm correspond to site A; the lines at 528.18, 528.55, and 529.18 nm correspond to site B; and the lines 528.59, 528.74, and 528.80 nm correspond to site C. The line positions for both the $^7F_0 \rightarrow {}^5D_0$ and $^7F_0 \rightarrow {}^5D_1$ excitation spectra of the nanocrystalline material reveal a small shift toward shorter wavelengths (<1 nm) compared to those of the bulk material. The most noticeable difference in the spectra is that the spectral lines of the nanocrystals are much broader than those of the bulk material. All excitation spectra were recorded by monitoring fluorescence using a low-resolution monochromator with a 6 nm band-pass. This wide band-pass prevents selective monitoring of only portions of the fluorescence lines and provides a reasonably good measure of the inhomogeneous broadening in the excitation spectra. Since the fluorescence lifetimes of the nanocrystalline sample are not shorter than the lifetimes of the bulk material, the broadening in these spectra is attributed solely to inhomogeneous broadening caused by disorder. Although not obvious in these spectra, increasing the sensitivity of the spectra reveal weak broad lines at approximately 580 nm ($^7F_0 \rightarrow {}^5D_0$) and 526.5 nm ($^7F_0 \rightarrow {}^5D_1$) in the nanocrystalline sample. These broad lines increase in intensity as the particle size decreases and become dominant for ~5 nm diameter particles.[7] No trace of these new lines was observed in the spectra of the bulk material.

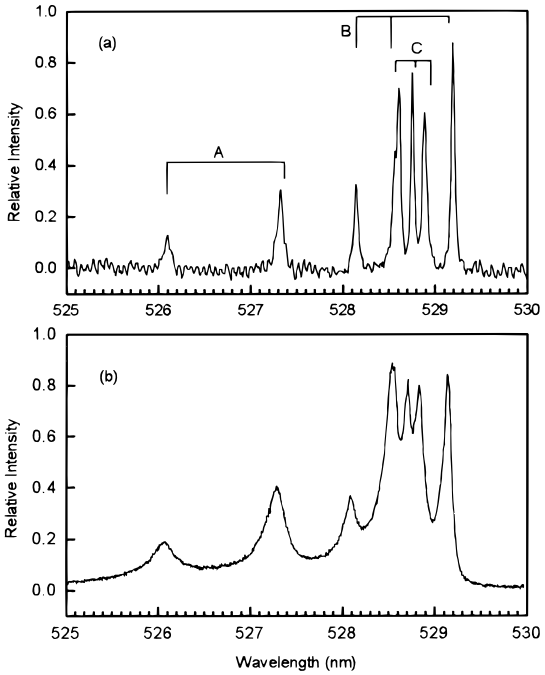

Figure 5. $^7F_0 - {}^5D_1$ excitation spectra of (a) bulk monoclinic 0.1% Eu^{3+}:Y_2O_3 and (b) nanocrystalline 0.1% Eu^{3+}:Y_2O_3. The 0.25 m monochromator was set at 624.1 nm, and the boxcar delay and gate width were 20 μs and 150 μs, respectively.

Site-selective fluorescence spectra were recorded by tuning the laser to a specific wavelength for a site and scanning the 1 m monochromator. Figure 6 shows fluorescence spectra of bulk monoclinic Eu^{3+}:Y_2O_3 when exciting a $^5D_1$ level for sites A, B, and C. The lines clustered near 590 nm are due to $^5D_1 \rightarrow {}^7F_3$ and $^5D_1 \rightarrow {}^7F_{0,1}$ transitions, and the lines clustered near 620 nm are due to $^5D_1 \rightarrow {}^7F_4$ and $^5D_0 \rightarrow {}^7F_2$ transitions. The fluorescence lines originating from $^5D_1$ and $^5D_0$ can be distinguished by their very different temporal behavior. This paragraph discusses the $^5D_0 \rightarrow {}^7F_{0,1}$ transitions in these spectra, and the following paragraph discusses the $^5D_0 \rightarrow {}^7F_2$ spectra in more detail. The $^5D_1 \rightarrow {}^7F_3$ and $^5D_1 \rightarrow {}^7F_4$ lines were not

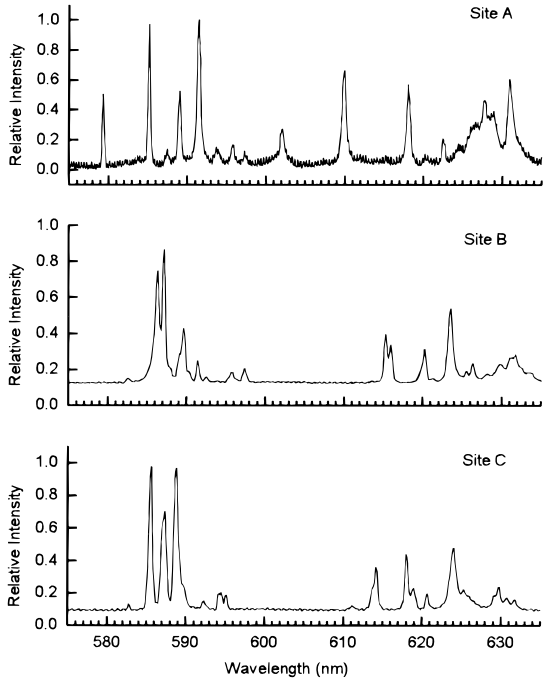

Figure 6. Fluorescence spectra of bulk monoclinic 0.1% Eu^{3+}:Y_2O_3 exciting the $^5D_1$ level. The excitation wavelengths were 527.31, 529.18, and 528.74 nm for sites A, B, and C, respectively. The boxcar delay and gate widths were 1 and 150 μs, respectively, and the band-pass of the 1 m monochromator was 0.2 nm.

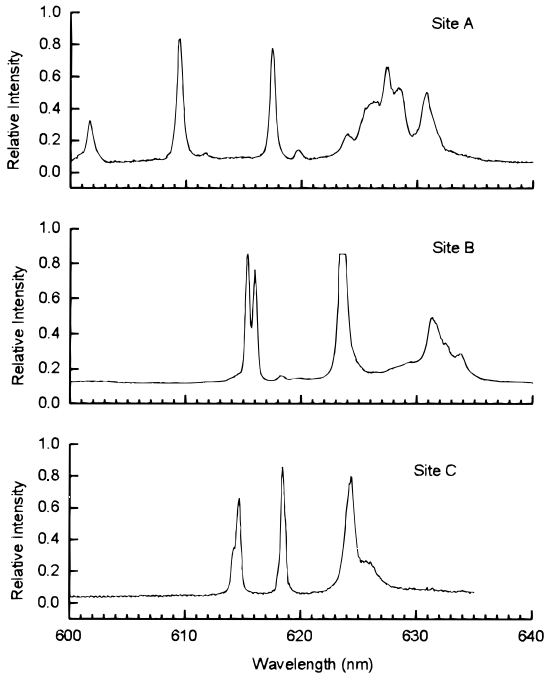

Figure 7. $^5D_0 \rightarrow {}^7F_2$ fluorescence spectra of bulk monoclinic 0.1% Eu^{3+}:Y_2O_3. The excitation wavelengths were 579.39, 582.72, and 582.87 nm for sites A, B, and C, respectively. The boxcar delay and gate widths were 1 and 150 μs, respectively, and the band-pass of the 1 m monochromator was 0.2 nm.

investigated in detail. Exciting site A resulted in fluorescence lines of weak intensity for the $^5D_1$ transitions at 587.46, 589.03, and 593.94 nm. Site B excitation produced sharp fluorescence lines at 586.71, 587.50, and 623.71 nm. The 586.71 and 587.50 nm lines correspond to $^5D_1 \rightarrow {}^7F_3$ transitions. Excitation of site C revealed sharp fluorescence lines at 585.71, 588.81, 589.01, and 624.52 nm and several other lines of weaker intensity. The lines at 585.71 and 588.81 correspond to $^5D_1 \rightarrow {}^7F_3$ transitions. A distinct difference in the spectra of site A compared to sites B and C is a relatively intense $^5D_0 \rightarrow {}^7F_0$ fluorescence line. This transition in nominally forbidden, and is usually quite weak. The fluorescence dynamics (discussed below) suggest that site A has a stronger electron−phonon coupling than sites B and C, and the strong $^5D_0 \rightarrow {}^7F_0$ fluorescence of site A is consistent with that supposition.

Figure 7 shows the $^5D_0 \rightarrow {}^7F_2$ fluorescence spectra of bulk monoclinic Eu^{3+}:Y_2O_3 when exciting the $^5D_0$ level of sites A, B, and C. The fluorescence spectrum of site A had an intensity lower than that of sites B and C spectra, and it also had more lines than expected for the $^5D_0 \rightarrow {}^7F_2$ transition. On the basis of the number of site A lines in Figure 6, the fluorescence line at 601.9 nm can be assigned as a $^5D_0 \rightarrow {}^7F_1$ transition. The lines at 609.7, 617.7, 627.7, and 630.6 nm are strong and sharp and can be assigned as $^5D_0 \rightarrow {}^7F_2$ transitions. The other features in the spectrum appear as broad or weak shoulders and are probably vibronic bands or satellite lines. The only difference between these assignments and the work on monoclinic Eu^{3+}:Gd_2O_3 is that the 631.0 nm in Eu^{3+}:Gd_2O_3 was assigned as a vibronic sideband.[18] The fluorescence spectrum of site B has sharp lines at 615.5, 616.2, and 623.7 nm and a broad, structured feature at 631.4 nm. The fluorescence spectrum of site C has sharp lines at 614.8, 618.7, and 624.6 nm and a shoulder at 626.2 nm. The line at 614.8 nm appears to be an unresolved doublet, which would be consistent with the calculated spectrum in ref 18. The fluorescence spectra of the bulk material show no indication of energy transfer between the different sites. In the nanocrystals, energy transfer was observed from site A to sites B and C.[8] The energy transfer in the nanocrystals probably indicate that either the overall or the local concentration of the dopant was higher than 0.1%.

TABLE 1: Fluorescence Lifetimes of Monoclinic 0.1% Eu^{3+}:Y_2O_3

	site A	site B	site C
$^5D_1$			
bulk	71 ± 7 μs	112 ± 6 μs	138 ± 7 μs
nanocrystal	45 ± 7 μs	117 ± 9 μs	156 ± 8 μs
$^5D_0$			
bulk	1.57 ± 0.07 ms	0.78 ± 0.04 ms	0.82 ± 0.04 ms
nanocrystal	1.75 ± 0.12 ms	1.32 ± 0.09 ms	1.32 ± 0.06 ms

Fluorescence decay lifetimes were obtained by selectively exciting and monitoring specific lines for each site. The lifetime values reported for each site are the average of measurements recorded when monitoring different fluorescence lines. Direct excitation of the $^5D_0$ level of the bulk material resulted in single-exponential lifetimes of 1.57, 0.78, and 0.82 ms, for sites A, B, and C, respectively. Table 1 summarizes the lifetimes obtained from the fluorescence decay transients of both the bulk and nanocrystalline material. For the $^5D_0$ level, the lifetimes for all sites are shorter in the bulk material. The decay time of the site A $^5D_0$ level is longer than that of sites B and C, and this qualitative trend is similar in bulk Eu^{3+}:Y_2O_3, nanocrystalline Eu^{3+}:Y_2O_3, and Eu^{3+}:Gd_2O_3.[18]

The $^5D_1$ decay times for sites B and C were measured by monitoring $^5D_1 \rightarrow {}^7F_3$ fluorescence in the 585−602 nm spectral range. These lifetimes were obtained from a single-exponential fit to the data. The $^5D_1$ fluorescence decay times for sites B and C in the bulk material were 112 and 138 μs, respectively. The directly excited $^5D_1$ fluorescence of site A did not appear to be a single exponential, but the signal was too weak to obtain a good fit. The $^5D_1$ decay time for site A was obtained by monitoring $^5D_0$ fluorescence after exciting the $^5D_1$ levels. These transients were fit to the function $(e^{-t/\tau_1} - e^{-t/\tau_2})$, where τ_1 and

τ_2 are the $^5D_0$ and $^5D_1$ lifetimes, respectively. The results of these fits gave a $^5D_0$ lifetime that was the same as that when measured directly and $^5D_1$ lifetime of 71 μs for site A.

4. Summary

These optical results on bulk monoclinic Eu^{3+}:Y_2O_3 provide reference spectra and excited-state lifetimes that allow evaluation of the optical properties of Eu^{3+}:Y_2O_3 nanocrystals. The anomalies of site A, such as the additional lines in the $^5D_0 \rightarrow {}^7F_2$ fluorescence spectra, observed in the nanocrystalline material are also present in the bulk material and are attributed to intrinsic features of the monoclinic phase of Eu^{3+}:Y_2O_3. The broad-band excitation spectra of 23 nm 0.1% Eu^{3+}:Y_2O_3 show only small shifts in line positions but a significant increase in the inhomogeneous broadening compared to the spectra of the bulk material. The excitation spectra of Eu^{3+}:Y_2O_3 nanocrystals also contained weak broad features that increased in intensity as the particle size decreased.[7] These broad lines are completely absent in the bulk material and are therefore attributed to a different "phase" in the nanocrystalline samples.

Energy transfer was observed from site A to sites B and C in the nanocrystals, but not in the bulk material. This observation suggests a difference in the total dopant concentration or a difference in the dopant distribution between the bulk and nanocrystalline samples. The $^5D_0$ and $^5D_1$ fluorescence lifetimes of sites A, B, and C show the same qualitative trends in both the bulk and nanocrystalline materials. There is no significant shortening of the $^5D_0$ fluorescence lifetimes due to quenching by surface effects in the nanocrystalline material. In fact, with the exception of the $^5D_1$ lifetime of site A, the lifetimes are the same or longer in the nanocrystals compared to those in the bulk material. A lengthening of the (non-single-exponential) fluorescence transient was also observed when the particle diameter of Eu_2O_3 decreased from 18 to 12 nm.[25] Now that the fluorescence properties of bulk monoclinic Eu^{3+}:Y_2O_3 are known, the fluorescence dynamics of Eu^{3+}:Y_2O_3 and Eu_2O_3 can be investigated as a function of particle size, annealing, etc., to study the defect chemistry, phonon behavior, and electron−phonon coupling of dopants in nanometer-size particles.

Acknowledgment. We are grateful to Professor A. Navrotsky at Princeton University for providing the use of the high-pressure, high-temperature synthesis equipment. This work was supported by the National Science Foundation (CAREER award CHE-9502460) and by a Research Corporation Cottrell Scholars Award.

References and Notes

(1) Maestro, P.; Huguenin, D. *J. Alloys Compd.* **1995**, 225, 520.
(2) Li, Z.; Hahn, H.; Siegel, R. W. *Mater. Lett.* **1988**, *6*, 342.
(3) Andres, R. P.; Averback, R. S.; Brown, W. L.; Brus, L. E.; Goddard, W. A., III; Kaldor, A.; Louie, S. G.; Moscovits, M.; Peercy, P. S.; Riley, S. J.; Siegel, R. W.; Spaepen, F.; Wang, Y. J. *Mater. Res.* **1989**, *4*, 704.
(4) Hadjipanayis, G. C.; Siegel, R. W., Eds.; *Nanophase Materials: Synthesis Properties Applications;* NATO ASI Series E 260, Kluwer: Dordrecht, 1993.
(5) Gleiter, H. *Prog. Mater. Sci.* **1989**, *33*, 223.
(6) Hase, T.; Kano, T.; Nakazawa, E.; Yamamoto, H. *Adv. Electron. Electron Phys.* **1990**, *79*, 271.
(7) Eilers, H.; Tissue, B. M. *Chem. Phys. Lett.* **1996**, *251*, 74.
(8) Bihari, B.; Eilers, H.; Tissue, B. M. *J. Lumin.* **1997**, *75*, 1.
(9) Goldburt, E. T.; Kulkarni, B.; Bhargava, R. N.; Taylor, J.; Libera, M. *J. Lumin.* **1997**, *72*−*74*, 190.
(10) Tao, Y.; Zhao, G.; Ju, X.; Shao, X.; Zhang, W.; Xia, S. *Mater. Lett.* **1996**, *28*, 137.
(11) Skandan, G.; Foster, C. M.; Frase, H.; Ali, M. N.; Parker, J. C.; Hahn, H. *Nanostruct. Mater.* **1992**, *1*, 313.
(12) Eilers, H.; Tissue, B. M. *Mater. Lett.* **1995**, *24*, 261.
(13) Eyring, L. *Handbook on the Physics and Chemistry of Rare Earths;* Gschneidner, K. A., Jr.; Eyring, L., Eds.; North-Holland: Amsterdam, 1979; Vol. 3, p 337.
(14) Hoekstra, H. R. *Inorg Chem.* **1966**, *5*, 754.
(15) Chen, G.; Stump, N. A.; Haire, R. G.; Peterson, J. R. *J. Alloys Compd.* **1992**, *181*, 503.
(16) Hintzen, H. T.; van Noort, H. M. J. *Phys. Chem. Solids* **1988**, *49*, 873.
(17) Yakel, H. L. *Acta Crystallogr.* **1979**, *B35*, 564.
(18) Dexpert-Ghys, J.; Faucher, M.; Caro, P. *Phys. Rev. B* **1981**, *23*, 607.
(19) Milora, J.; Tissue, B. M. Unpublished results.
(20) Sheng, K. C.; Korenowski, G. M. *J. Phys. Chem.* **1988**, *92*, 50.
(21) Rice, D.; de Shazer, L. *J. Chem. Phys.* **1970**, *52*, 172.
(22) Vogt, G. *Proc. Electrochem. Soc.* **1988**, *5*, 572.
(23) Doss, J.; Zallen, R. *Phys. Rev. B.* **1993**, *48*, 15626 and references therein.
(24) Dieke, G. H. *Spectra and Energy Levels of Rare Earth Ions in Crystals*; Interscience: New York, 1968.
(25) Bihari, B.; Tissue, B. M. Unpublished results.